

Article

An Aggregation-Induced Fluorescence Probe for Detection H₂S and Its Application in Cell Imaging

Xin-Hui Tang *, Hao-Na Zhang, Wen-Ling Wang and Qing-Ming Wang * 

School of Pharmacy, Yancheng Teachers University, Yancheng 224051, China;
zhanghaonana2004@163.com (H.-N.Z.); wangwl@yctu.edu.cn (W.-L.W.)

* Correspondence: xinhuitang@sina.com (X.-H.T.); wangqm@yctu.edu.cn (Q.-M.W.)

Abstract: Monitoring hydrogen sulfide (H₂S) in living organisms is very important because H₂S acts as a regulator in many physiological and pathological processes. Upregulation of endogenous H₂S concentration has been shown to be closely related to the occurrence and development of tumors, atherosclerosis, neurodegenerative diseases and diabetes. Herin, a novel fluorescent probe **HND** with aggregation-induced emission was designed. Impressively, **HND** exhibited a high selectivity, fast response (1 min) and low detection limit (0.61 μM) for H₂S in PBS buffer (10 mM, pH = 7.42). Moreover, the reaction mechanism between **HND** and H₂S was conducted by Job's plot, HR-MS, and DFT. In particular, **HND** was successfully employed to detect H₂S in HeLa cells.

Keywords: aggregation-induced emission; fluorescent probe; hydrogen sulfide; cell imaging

1. Introduction

H₂S is considered to be an important endogenous gaseous transmitter and plays a crucial role in the regulation of intracellular redox status, angiogenesis and anti-inflammatory effects in living organisms [1–3]. It is generated from L-cysteine or catalyzed by cysteine sulfide β-synthases and cysteine sulfide γ-lyase [4]. Evidence showed that the upregulation of H₂S concentration is closely related to the occurrence and development of tumors, atherosclerosis, neurodegenerative diseases, diabetes and so on [5–9]. Therefore, it is necessary to construct a new H₂S instantaneous detection method with high sensitivity and selectivity to evaluate H₂S levels in biological systems.

Currently, many H₂S-activatable small-molecule fluorescent probes have been developed based on different reaction mechanisms, such as the removal of copper ion via copper sulfide precipitation, nucleophilic addition or the reduction of azides/or nitros to amines mediated by the thiolysis of dinitrophenyl ether [7,10–15]. However, some of them are based on hydrophobic organic fluorescent groups, which have the disadvantage of poor water solubility and easy aggregation to form precipitates in aqueous solutions, thereby reducing the responsivity to the analyte and limiting the practical application of organic fluorescent molecular probes in biological imaging. Due to the advantages of excellent photostability and biocompatibility of aggregation-induced emission (AIE), a lot of fluorescent probes with AIE effect for H₂S have been synthesized. However, most of the fluorescent probes with AIE effect are based on the molecular skeleton of tetrastylene (TPE) [16,17] and have relatively complex molecular structures, which increases the difficulty of AIE molecular design and synthesis. Therefore, the design of efficient AIE bioluminescent materials with simple molecular structures and simple synthesis remains a challenge.

In this paper, a novel AIE activity fluorescent probe, named 2-hydroxy-1-naphthaldehyde N-(dimethylamino)benzaldehyde (**HND**) was conducted. The mechanism was tested by Job's plot, HR-MS, and DFT, and revealed that the two C=N double bonds in the structure of **HND** were used to provide a receptor unit for H₂S. Compared with early reports (Table S1), **HND** exhibits a comparable limit of detection and a fast response. Furthermore, **HND** realized the detection of H₂S in HeLa cells.



Citation: Tang, X.-H.; Zhang, H.-N.; Wang, W.-L.; Wang, Q.-M. An Aggregation-Induced Fluorescence Probe for Detection H₂S and Its Application in Cell Imaging. *Molecules* **2024**, *29*, 2386. <https://doi.org/10.3390/molecules29102386>

Academic Editor: Haidong Li

Received: 26 April 2024

Revised: 13 May 2024

Accepted: 14 May 2024

Published: 19 May 2024



Copyright: © 2024 by the authors. Licensee MDPI, Basel, Switzerland. This article is an open access article distributed under the terms and conditions of the Creative Commons Attribution (CC BY) license (<https://creativecommons.org/licenses/by/4.0/>).

2. Results and Discussion

2.1. AIE Effect of HND in Solution

To better understand the AIE effect of HND, the fluorescence properties of HND in a mixed solvent system of DMSO and H₂O were first investigated. As an exception, HND showed no fluorescence signal when dissolved in the good solvent DMSO, while the fluorescence signal at 536 nm could be turned on and gradually increased with the increase in water volume fraction; an 8.23-fold increase was observed when the water volume fraction increased to 60% (as shown in Figure 1a). With the water volume fraction increased from 60% to 100%, the fluorescence signal reduced slightly. The photographs given in Figure 1d show the color change in HND with increasing water content. A clear yellow fluorescence was observed under a 365 nm lamp. These results indicated that the compound HND is a typical aggregation-induced emission (AIE) active compound in the aqueous medium [18]. Herein, DMSO is a good solvent and water is a poor solvent for HND [19]. The reason for the fluorescence enhancement of HND in DMSO is because the radiation channel was opened, leading to an increase in fluorescence intensity due to the restricted intramolecular rotations (RIRs) of the coumarin matrix and thiosemicarbazide [20].

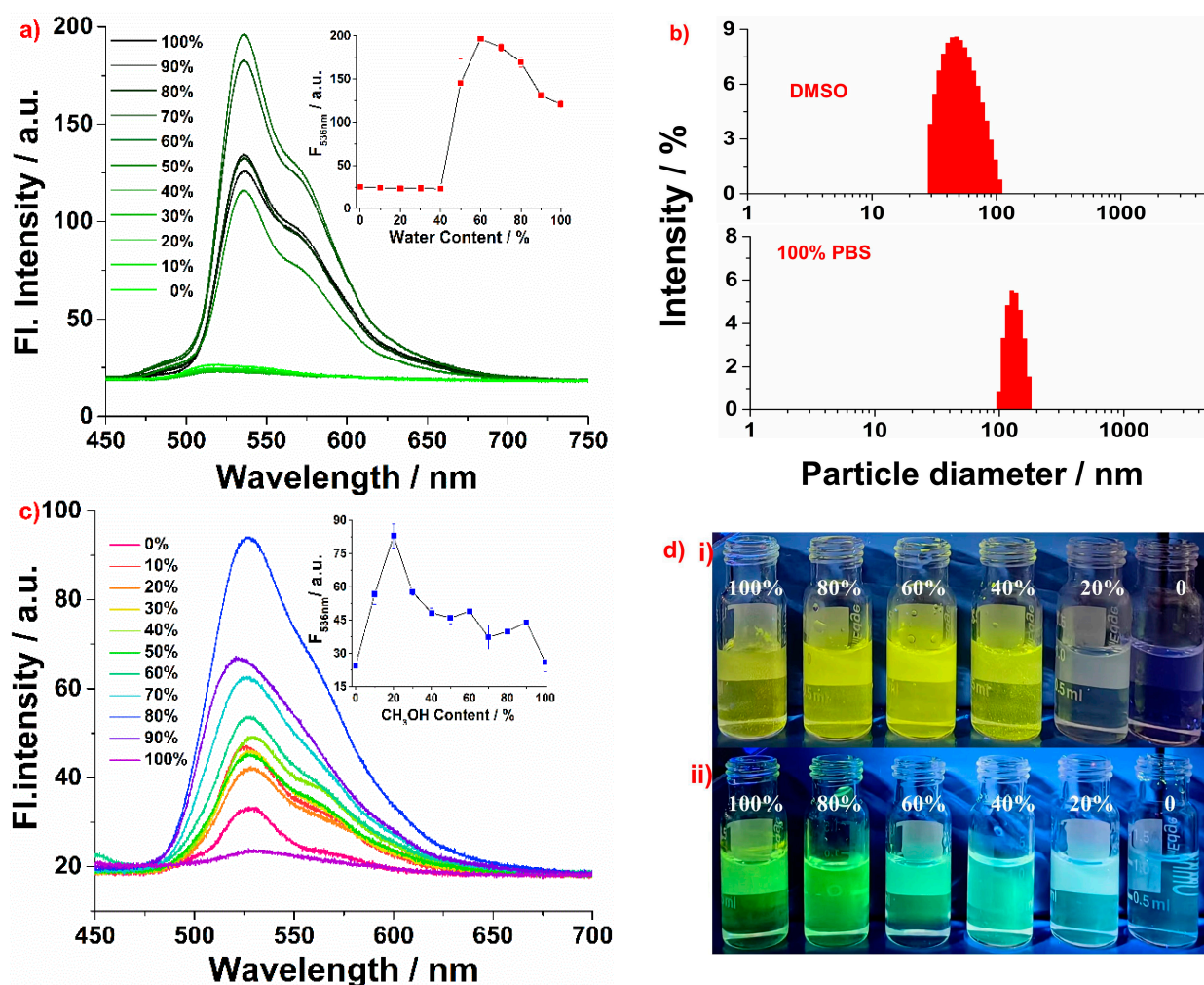


Figure 1. (a) Fluorescence spectra of HND (5.0 μM) in DMSO/water mixtures with different water fractions, pH 7.4. (b) Particle size analysis of HND in DMSO and PBS. (c) Fluorescence spectra of HND (5.0 μM) in CH₃OH/glycerin mixtures with different glycerin fractions, λ_{ex} = 420 nm. (d) The corresponding fluorescence images of HND under 365 nm UV lamp illumination ((i) different PBS/DMSO mixtures; (ii) different CH₃OH/glycerin mixtures).

Particle size analysis was a useful method to further verify the formation of aggregates of **HND**. As shown in Figure 1b, the average particle size of **HND** (5.0 μM) in DMSO solution was 45.69 nm, while the average diameter in PBS (10 mM, pH = 7.40) was approximately 128.52 nm, indicating that **HND** does indeed have aggregates in aqueous solutions. Furthermore, the diameter of **HND** was supplemented by transmission electron microscopy (TEM). The TEM results showed that the particle size of **HND** is approximately 100 nm, which is consistent with the results of particle size analysis (128.52 nm). In addition, TEM showed that the morphology of **HND** was almost elliptical and it had a structural feature with a darker color in the center and a thin film coating at the periphery (Figure S4).

To better understand the properties of AIE, we conducted analyses of the fluorescence spectra of **HND** (5.0 μM) in different CH_3OH /glycerin mixtures. As shown in Figure 1c, the fluorescence intensity at 536 nm increased with the increase in glycerol fractions. The results indicated that the sticky glycerin could block the nonradiative intramolecular rotation [18]. This means that **HND** is a typical AIE compound [13,19].

2.2. Selectivity and Competition

Many H_2S probes based on nucleophilic addition reaction have been reported in recent years [15,21–24]. To identify the interaction between **HND** and H_2S (Na_2S was employed as H_2S donor), as shown in Figure 2a, an extremely strong yellow fluorescence with $\lambda_{\text{max}} = 536 \text{ nm}$ was observed in PBS buffer solution (10 mM, pH = 7.40). However, the fluorescence intensity of **HND** (5.0 μM) was dramatically reduced after the addition of 100 eq. H_2S in PBS buffer solution (10 mM, pH = 7.40). The fluorescence intensity of **HND** was decreased to almost no fluorescence. There are other biologically relevant reactive sulfurs (RSS), such as Na_2SO_4 , Na_2SO_3 , NaHSO_4 , NaHSO_3 , $\text{Na}_2\text{S}_2\text{O}_3$, L-Cys and GSH, which could react with **HND**; here, it is necessary to verify the specificity of **HND**. In addition, many anions and cations, such as PO_4^{3-} , HCO_3^- , NO_2^- , Br^- , NO_3^- , F^- , CO_3^{2-} , Cl^- , $\text{C}_2\text{O}_4^{2-}$, I^- , etc., were also investigated. The results indicated that no detectable responses were observed when 100 eq. of other RSS or many anions were added to **HND**, respectively. The response of **HND** to H_2O_2 was also conducted; it was found that H_2O_2 could not respond to **HND**.

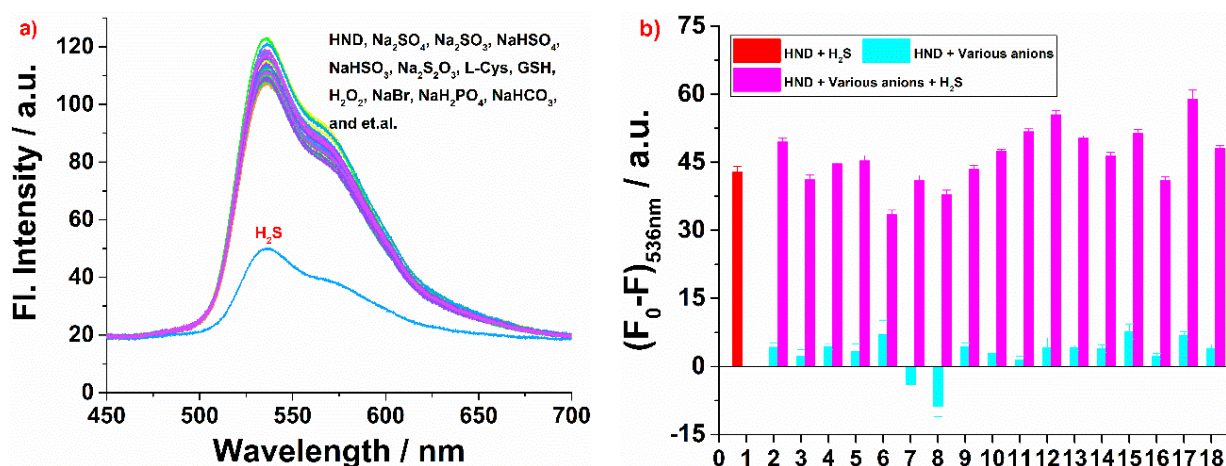


Figure 2. (a) Selectivity profile of 5.0 μM **HND** toward the RSS, various anions and H_2O_2 (500 μM) in PBS buffer (10 mM, pH 7.4), $\lambda_{\text{ex}} = 420 \text{ nm}$. (b) Fluorescence intensity changes of 5.0 μM **HND** upon addition of 100 equiv. H_2S and 100 equiv. of the RSS, various anions and H_2O_2 , $\lambda_{\text{em}} = 536 \text{ nm}$ (1–18: **HND**, $\text{Na}_2\text{S}_2\text{O}_3$, NaHSO_3 , Na_2SO_4 , Na_2SO_3 , L-Cys, GSH, H_2O_2 , Na_3PO_4 , NaI, NaF, NaCl, NaBr, Na_2CO_3 , NaHCO_3 , $\text{Na}_2\text{C}_2\text{O}_4$, NaNO_3 , NaNO_2).

In addition, a lot of metal ions, such as Mn^{2+} , Cu^{2+} , Ag^+ , Co^{3+} , Fe^{3+} , Al^{3+} , Ca^{2+} , K^+ , Ni^{2+} , Cd^{2+} , Cr^{3+} and so on, which coexist in the human body, were also investigated; except for Cu^{2+} , all other tested metal ions have no interference with **HND** (Figures S5 and S6). All of the results showed that **HND** has high selectivity for H_2S .

To further demonstrate the ability of **HND** to respond to H_2S in the presence of other biologically relevant reactive RSS, anions and H_2O_2 , the competition of **HND** was also examined (Figure 2b). It was found that **HND** could also respond to H_2S in the presence of other biologically relevant reactive RSS, anions and H_2O_2 , and the fluorescence intensity was similar to that of **HND** directly responding to H_2S . This informed us that the RSS, anions and H_2O_2 tested had a negligible interfering effect on the detection of H_2S by **HND**. Similarly, when metal ions and H_2S coexisted, the decrease in fluorescence intensity of **HND** was also observed (Figure S6).

2.3. H_2S Response by Probe **HND**

Figure 3a shows the relationship between **HND** and the concentrations of H_2S . The fluorescence intensity of **HND** in PBS buffer solution (10 mM, pH = 7.40) at 536 nm decreased with the gradual addition of H_2S at different concentrations. When 435 μM H_2S was added, a 5.71-fold quenching of the fluorescence was observed. The fluorescence color changed from light yellow to colorless (shown in Figure 3a inset). A good linear relationship was observed between the fluorescence intensities at 536 nm, as well as the H_2S concentration from 25 to 210 μM ; moreover, the value of the linear correlation R^2 was 0.9862 (Figure 3a inset). Followed by the equation $\text{LOD} = K \times \text{Sb1}/S$ [25], the detection limit for H_2S was estimated to be 0.61 μM . Compared with the early results (as shown in Table S1), the LOD value is consistent with the reports by Lu and Jose [26–28] and good compared with the reports by Zhang [29,30]. Additionally, the pH-dependent responses of probe **HND** and **HND** to H_2S were carried out. From Figure S7, it can be seen that probe **HND** could only respond to H_2S at pH 7.42. At other pH values, such as 4.00, 6.86, 9.18 and 10.01, **HND** could not respond to H_2S . Therefore, PBS buffer (10 mM, pH 7.4) was chosen as the reaction system.

CIE chromaticity was used to better understand the chromaticity changes in the fluorescence spectra of **HND** upon the addition of H_2S [31]. CIE chromaticity coordinates were also calculated from the emission spectrum [32]. A two-dimensional space (XY plane) could be found in the CIE where each point of the chromaticity map stands for a particular color. From Figure 3b, the CIE chromaticity of **HND** was found to be $x = 0.3818$, $y = 0.5219$, while after the addition of H_2S , the CIE chromaticity was converted to be $x = 0.3618$, $y = 0.4174$. This is an indication of a gradual shift in the color (Figure S8).

Response time is one of the most important parameters for a sensor. Therefore, kinetic studies were conducted to investigate the response time. A total of 10 equiv. of H_2S was added to **HND** (5.0 μM) and the fluorescence intensity at 536 nm was monitored over time until the spectrum became constant (Figure 3c). The results showed that it takes almost 1 min for **HND** to react completely with H_2S . This is a fast reaction rate compared to the first report [13,28,33,34].

Furthermore, the absorption spectra of **HND** (15 μM) treated with different concentrations of H_2S in PBS buffer solution (10 mM, pH = 7.40) were recorded. As shown in Figure 3d, four peaks at 457 nm, 427 nm, 404 nm and 355 nm were observed; with the addition of H_2S , the peaks at 457 nm, 427 nm, 404 nm and 355 nm were decreased and two new peaks at 438 nm and 326 nm appeared and gradually increased. An isoabsorption point at 329 nm was found. The isoabsorptive point indicated that a new compound was formed between **HND** and H_2S [31,35].

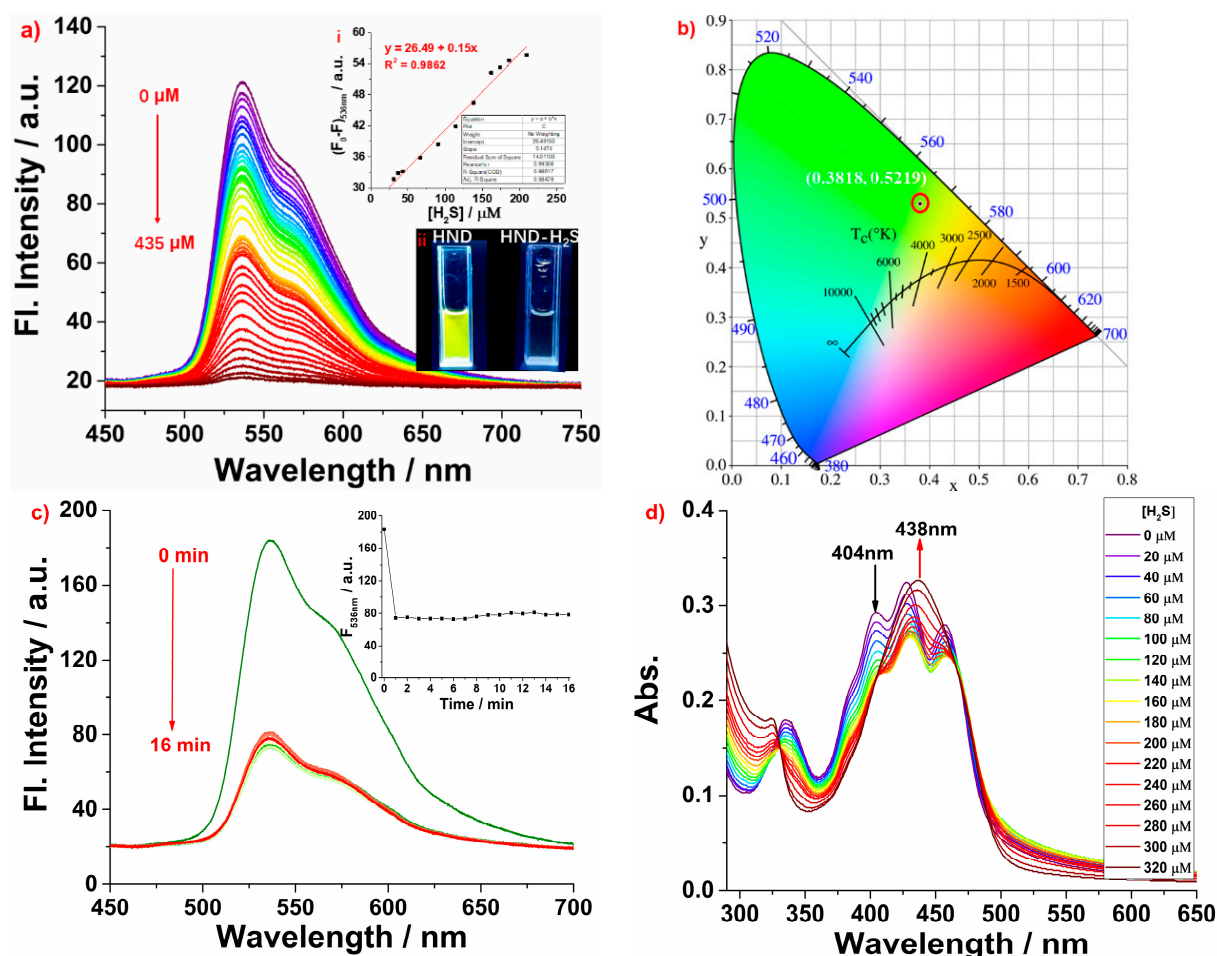


Figure 3. (a) The fluorescence titration curve of 5.0 μM HND in the presence of different concentrations of H₂S. Inset: (i) The corresponding fluorescence images of HND and HND mixed with H₂S under 365 nm UV lamp illumination. (ii) Changes in emission intensity at 536 nm with incremental additions of H₂S. (b) CIE diagram of the HND in PBS buffer solution (10 mM, pH = 7.40). (c) Changes in emission intensity of HND (5.0 μM) at 536 nm in the presence of 10 equiv. of H₂S as the function of time. (d) Absorption spectra of HND (15 μM) treated with different concentrations of H₂S.

2.4. Mechanism Investigation

HR-MS was used to further investigate the mechanism involved in the fluorescence quenching between HND and Na₂S. The HR-MS of HND shows a strong peak at $m/z = 318.1606$ [HND + H]⁺ (Figure S2). After the addition of an excess of Na₂S, a new peak appears at $m/z = 418.1619$ [HND -HS + CH₃OH + H]⁺, which indicates clearly that the C=N of HND were formed through nucleophilic addition by H₂S in aqueous solution (Figure 4). The recognition mechanism is similar to the other reports [36–39].

DFT with B3LYP/6-31G(d) (the Gaussian 09) was carried out to further investigate the electron distributions and orbital energies of HND and H₂S [40,41]. From Figure 5, we find that the highest occupied molecular orbitals (HOMOs) and the lowest occupied molecular orbitals (LOMOs) of HND were mainly distributed over the whole molecule, so HND showed a strong fluorescence due to the absence of electron transfer. The HOMOs and LUMOs of HND -HS were mainly distributed on the 2-hydroxy-1-naphthylaldehyde group. The HOMO-LUMO energy gaps of HND and HND -HS were 9.1417 eV and 10.3809 eV, respectively. The HOMO-LUMO band gap of HND -HS was higher than that of HND, which could be clearly explained by the blue shift in the emission maxima of HND -HS [32,42].

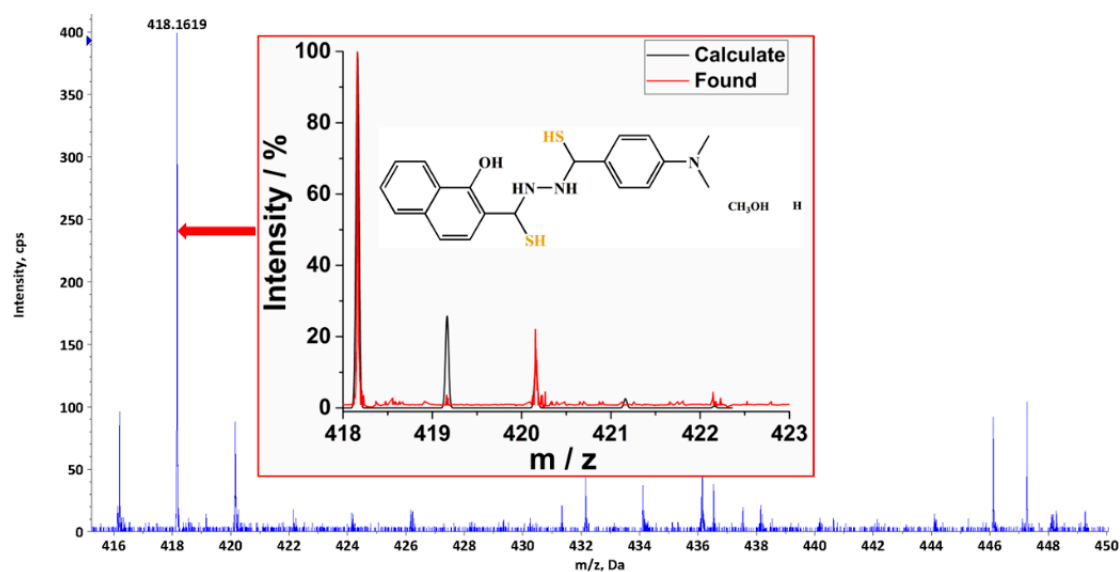


Figure 4. ESI mass spectrum of HND upon addition of excess Na_2S .

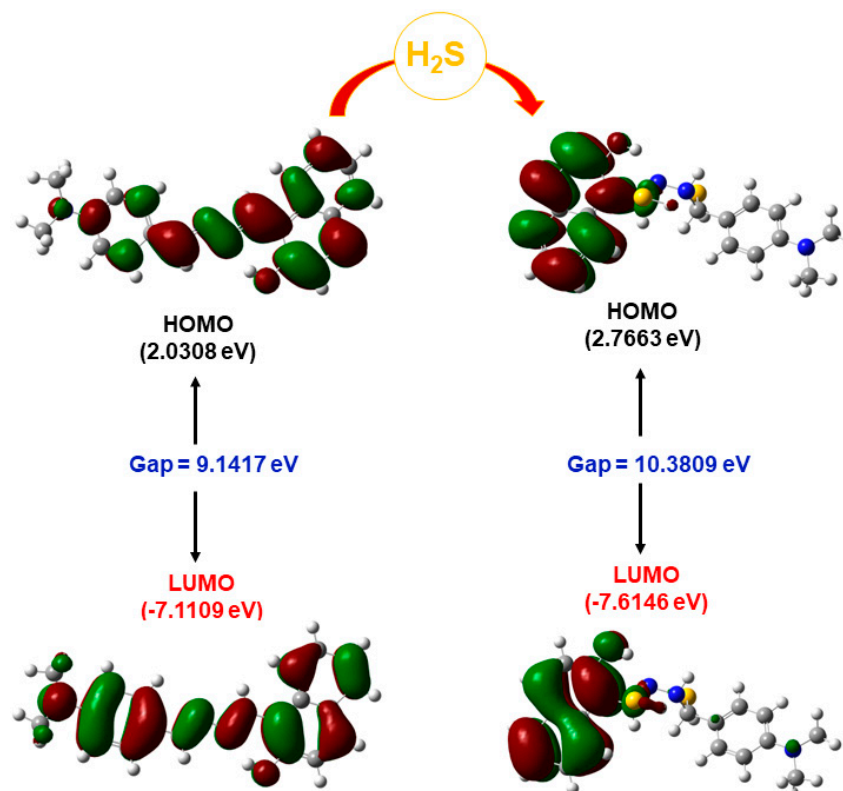


Figure 5. HOMOs and LUMOs of HND and HND-HS.

2.5. Fluorescence Imaging

The applicability of HND in biological systems was investigated by analyzing H_2S imaging in living cells. Bright yellow fluorescence was obtained when HeLa cells were incubated with $20 \mu\text{M}$ of HND for 20 min. However, the bright yellow fluorescence of HeLa cells was gradually quenched when the cells were treated with HND for 20 min and then treated with H_2S (the concentrations of H_2S were $20 \mu\text{M}$ and $40 \mu\text{M}$, respectively) for another 20 min (Figure 6b,c). The results indicated that HND has good biocompatibility and is able to image different concentrations of H_2S in living cells.

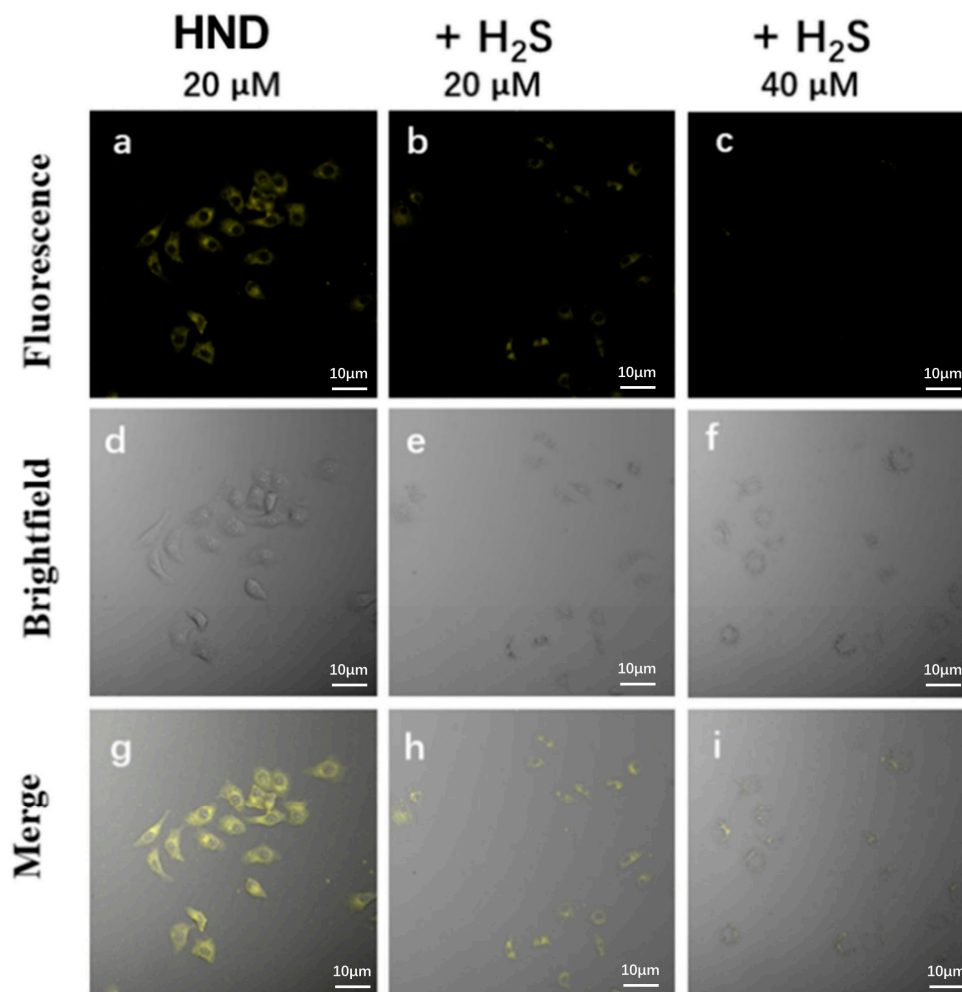


Figure 6. Fluorescence microscopy images of HeLa cells. (a,d,g) HeLa cells incubated with HND (20 μM) for 20 min. (b,e,h) HeLa cells pretreated with HND (20 μM) and then treated with H₂S (20 μM) for 20 min. (c,f,i) HeLa cells pretreated with HND (20 μM) and then treated with H₂S (40 μM) for 20 min.

3. Materials and Methods

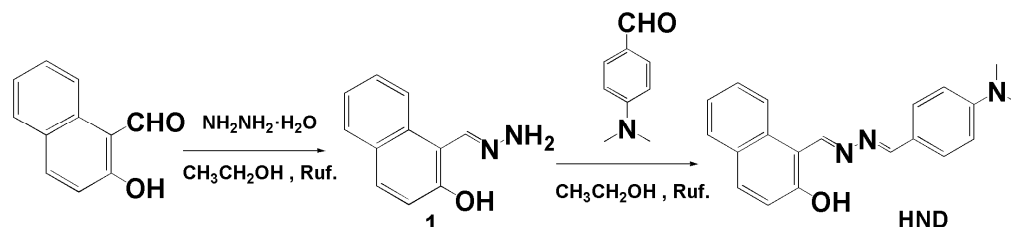
3.1. Materials

All reagents were purchased through a commercial method and used without further purification. ¹H-NMR was obtained using a Bruker DRX 400 spectrometer with TMS as the internal standard. High-resolution mass spectrometry (HR-MS) was performed on a Triple TOF TM 5600+ system. Fluorescence spectra were obtained at room temperature using a CRT-970 fluorescence spectrophotometer. The absorption spectra were measured by Shimadzu UV1800. Imaging of probe HND and HND with Na₂S was conducted on a confocal laser scanning microscope L700 with HeLa cells.

3.2. The Synthesis Process

As shown in Scheme 1, first, the mixture of ethanol (30 mL), 2-hydroxynaphthalene-1-carbaldehyde (0.344 g, 2.0 mmol) and hydrazine hydrate (400 μL) were first refluxed in a flask. After 10 h, the reaction was stopped by TLC. Yellow solids were obtained, named 2-hydroxynaphthalene-1-carbaldehyde hydrazone (1). Next, 1 (0.279 g, 1.5 mmol) and 4-(dimethylamino)benzaldehyde (0.1491 g, 1.0 mmol) were mixed in 30 mL ethanol, a few drops of DMF was added as a catalyst, and then the above mixture was heated and refluxed for 24 h. The yellow powder HND was obtained after the mixture was cooled and washed by ethanol three times; then, it was recrystallized by CH₃CH₂OH. Yield, 0.17 g

(54%). $^1\text{H-NMR}$ (400 MHz, $\text{DMSO-}d_6$) δ 12.90 (s, 1H), 10.01 (s, 1H), 8.66 (d, $J = 8.6$ Hz, 1H), 8.05 (d, $J = 8.9$ Hz, 1H), 7.93 (d, $J = 7.3$ Hz, 1H), 7.63 (t, $J = 7.7$ Hz, 1H), 7.45 (t, $J = 7.1$ Hz, 1H), 7.29 (d, $J = 9.0$ Hz, 1H), 1.23 (s, 6H) (Figure S1). HR-MS: $m/z = 318.1606$ [$\text{HND} + \text{H}$] $^+$, [$\text{HND} + \text{H}$] $^+$ found 318.1606 (Figure S2). **HND** showed the yellow fluorescence in the solid under 365 nm UV lamp illumination (Figure S3).



Scheme 1. Design and synthesis of the **HND**.

3.3. Fluorescence Spectral Property

Na_2S was dissolved in water and used as the donor of H_2S [36]. Stock solution of probe **HND** (10^{-3} M) was prepared in DMSO. The fluorescence spectra of **HND** with H_2S were obtained by the addition of various concentrations of Na_2S to **HND** ($5.0 \mu\text{M}$) in PBS buffer (10 mM, pH 7.4). The fluorescence spectra were excited by 420 nm.

4. Conclusions

In conclusion, a novel fluorescent probe **HND** with AIE activity was synthesized. The results showed that **HND** could be used for the detection of H_2S in aqueous solution and HeLa cells. **HND** exhibited obvious fluorescence quenching and excellent selectivity/competitiveness toward H_2S with a limit of detection of $0.64 \mu\text{M}$ and a response time of 1 min. We assumed that H_2S reacted with **HND** through nucleophilic addition reaction and the mechanism was proven by HR-MS and DFT calculations. In addition, **HND** was successfully applied to image the H_2S in HeLa cells.

Supplementary Materials: The following supporting information can be downloaded at: <https://www.mdpi.com/article/10.3390/molecules29102386/s1>, Figure S1: $^1\text{H-NMR}$ of **HND**. Figure S2: HR-MS of **HND**. Figure S3: The color of **HND** as a solid. (Right) under 365 nm UV lamp illumination; (left) under visible light. Figure S4: TEM of **HND** ($5.0 \mu\text{M}$) in 100% PBS. Figure S5: Selectivity profile of $5 \mu\text{M}$ **HND** toward various metal ions ($500 \mu\text{M}$) in PBS buffer (10 mM, pH 7.4), $\lambda_{\text{ex}} = 420$ nm. Figure S6: Fluorescence intensity changes of $5.0 \mu\text{M}$ **HND** upon addition of 100 equiv. H_2S and 100 equiv. of various metal ions, $\lambda_{\text{em}} = 536$ nm. Figure S7: The pH-dependent responses of probe **HND** and **HND** to H_2S . Figure S8: CIE diagram of the **HND**-**HS** in PBS buffer solution (10 mM, pH = 7.40). Figure S9: Time-dependent fluorescence intensity of **HND** ($5.0 \mu\text{M}$) in PBS (pH 7.4, 10 mM). Table S1: Comparison of **HND** for the detection of H_2S . References [43–45] are cited in Supplementary Materials.

Author Contributions: Data curation, X.-H.T. and H.-N.Z.; Investigation, X.-H.T. and H.-N.Z.; Data curation, W.-L.W.; Writing—original draft preparation, X.-H.T.; Writing—review and editing, Q.-M.W. All authors have read and agreed to the published version of the manuscript.

Funding: This research received no external funding.

Institutional Review Board Statement: Not applicable.

Data Availability Statement: The original contributions presented in the study are included in the article/supplementary material, further inquiries can be directed to the corresponding authors.

Acknowledgments: We would like to thank Cheng Yu from Hebei University of Science and Technology for his help with DFT.

Conflicts of Interest: The authors declare no conflicts of interest.

References

1. Yang, G.; Wu, L.; Jiang, B.; Yang, W.; Qi, J.; Cao, K.; Meng, Q.; Mustafa, A.K.; Mu, W.; Zhang, S.; et al. H₂S as a Physiologic Vasorelaxant: Hypertension in Mice with Deletion of Cystathionine γ -Lyase. *Science* **2008**, *322*, 587–590. [[CrossRef](#)] [[PubMed](#)]
2. Wallace, J.L. Hydrogen sulfide-releasing anti-inflammatory drugs. *Trends Pharmacol. Sci.* **2007**, *28*, 501–505. [[CrossRef](#)] [[PubMed](#)]
3. Li, Y.; Quan, W.; Song, W.; Zhan, J.; Lin, W. Near-infrared fluorescent probe for visualizing hydrogen sulfide fluctuations during arthritis and its treatment. *Microchem. J.* **2023**, *191*, 108856. [[CrossRef](#)]
4. Singh, S.; Padovani, D.; Leslie, R.A.; Chiku, T.; Banerjee, R. Relative Contributions of Cystathionine β -Synthase and γ -Cystathionase to H₂S Biogenesis via Alternative Trans-sulfuration Reactions. *J. Biol. Chem.* **2009**, *284*, 22457–22466. [[CrossRef](#)] [[PubMed](#)]
5. Yu, C.; Li, X.; Zeng, F.; Zheng, F.; Wu, S. Carbon-dot-based ratiometric fluorescent sensor for detecting hydrogen sulfide in aqueous media and inside live cells. *Chem. Commun.* **2013**, *49*, 403–405. [[CrossRef](#)]
6. Giuliani, D.; Ottani, A.; Zaffe, D.; Galantucci, M.; Strinati, F.; Lodi, R.; Guarini, S. Hydrogen sulfide slows down progression of experimental Alzheimer's disease by targeting multiple pathophysiological mechanisms. *Neurobiol. Learn. Mem.* **2013**, *104*, 82–91. [[CrossRef](#)] [[PubMed](#)]
7. Wang, B.; Wang, X.; Zeng, A.; Leng, J.; Zhao, W. Engineering a mitochondria-targeted ratiometric fluorescent probe with a large Stokes shift for H₂S-specific assaying in foodstuffs and living cells. *Sens. Actuators B Chem.* **2021**, *343*, 130095. [[CrossRef](#)]
8. Wu, L.; Ishigaki, Y.; Hu, Y.; Sugimoto, K.; Zeng, W.; Harimoto, T.; Sun, Y.; He, J.; Suzuki, T.; Jiang, X.; et al. H₂S-activatable near-infrared afterglow luminescent probes for sensitive molecular imaging in vivo. *Nat. Commun.* **2020**, *11*, 446. [[CrossRef](#)] [[PubMed](#)]
9. Yang, W.; Yang, G.; Jia, X.; Wu, L.; Wang, R. Activation of KATP channels by H₂S in rat insulin-secreting cells and the underlying mechanisms. *J. Physiol.* **2005**, *569*, 519–531. [[CrossRef](#)]
10. Chen, S.; Li, H.; Hou, P. A novel imidazo [1,5- α]pyridine-based fluorescent probe with a large Stokes shift for imaging hydrogen sulfide. *Sens. Actuators B Chem.* **2018**, *256*, 1086–1092. [[CrossRef](#)]
11. Wang, J.; Wen, Y.; Huo, F.; Yin, C. Based 'successive' nucleophilic substitution mitochondrial-targeted H₂S red light emissive fluorescent probe and its imaging in mice. *Sens. Actuators B Chem.* **2019**, *297*, 126773. [[CrossRef](#)]
12. Jin, L.; Tan, X.; Dai, L.; Bai, H.; Wang, Q. Modulation of fluorescence sensing properties of coumarin-based fluorescent probe for H₂S and its application in cell imaging. *Spectrochim. Acta A Mol. Biomol. Spectrosc.* **2019**, *221*, 117187. [[CrossRef](#)] [[PubMed](#)]
13. Zhao, B.; Yang, Y.; Wu, Y.; Yang, B.; Chai, J.; Hu, X.; Liu, B. To re-evaluate the emission mechanism, AIE activity of 5-azido fluorescein and its reaction with H₂S and NO. *Sens. Actuators B Chem.* **2018**, *256*, 79–88. [[CrossRef](#)]
14. Gunduz, H.; Almamnadov, T.; Dirak, M.; Acari, A.; Bozkurt, B.; Kolemen, S. A mitochondria-targeted chemiluminescent probe for detection of hydrogen sulfide in cancer cells, human serum and in vivo. *RSC Chem. Biol.* **2023**, *4*, 675–684. [[CrossRef](#)] [[PubMed](#)]
15. Zhu, T.; Ren, N.; Liu, X.; Dong, Y.; Wang, R.; Gao, J.; Sun, J.; Zhu, Y.; Wang, L.; Fan, C.; et al. Probing the Intracellular Dynamics of Nitric Oxide and Hydrogen Sulfide Using an Activatable NIR II Fluorescence Reporter. *Angew. Chem.* **2021**, *60*, 8450–8454. [[CrossRef](#)]
16. Zhu, A.; Ali, S.; Jiao, T.; Wang, Z.; Xu, Y.; Ouyang, Q.; Chen, Q. Facile synthesis of fluorescence-SERS dual-probe nanocomposites for ultrasensitive detection of sulfur-containing gases in water and beer samples. *Food Chem.* **2023**, *420*, 136095. [[CrossRef](#)]
17. Yu, H.; Ryu, K.; Park, J.; Subedi, S.; Lee, K.-H. Design and synthesis of fluorescent peptide-based probes with aggregation-induced emission characteristic for detecting CH₃Hg⁺ and Hg²⁺ in aqueous environment: Tuning fluorescent detection for CH₃Hg⁺ by replacing peptide receptors. *Dye. Pigment.* **2022**, *204*, 110461. [[CrossRef](#)]
18. Nicol, A.; Qin, W.; Kwok RT, K.; Burkhartsmeyer, J.M.; Zhu, Z.; Su, H.; Luo, W.; Lam JW, Y.; Qian, J.; Wong, K.S.; et al. Functionalized AIE nanoparticles with efficient deep-red emission, mitochondrial specificity, cancer cell selectivity and multiphoton susceptibility. *Chem. Sci.* **2017**, *8*, 4634–4643. [[CrossRef](#)]
19. Zhao, B.; Yang, B.; Hu, X.; Liu, B. Two colorimetric and ratiometric fluorescence probes for hydrogen sulfide based on AIE strategy of alpha-cyanostilbenes. *Spectrochim. Acta A Mol. Biomol. Spectrosc.* **2018**, *199*, 117–122. [[CrossRef](#)]
20. Fang, W.; Zhang, G.; Chen, J.; Kong, L.; Yang, L.; Bi, H.; Yang, J. An AIE active probe for specific sensing of Hg²⁺ based on linear conjugated bis-Schiff base. *Sens. Actuators B Chem.* **2016**, *229*, 338–346. [[CrossRef](#)]
21. Hou, J.; Huang, Y.; Fu, L.; Sun, M.; Wang, L.; Guo, R.; Chen, L.; Lv, C. Evaluating the Effect of Hydrogen Sulfide in the Idiopathic Pulmonary Fibrosis Model with a Fluorescent Probe. *Anal. Chem.* **2023**, *95*, 5514–5521. [[CrossRef](#)] [[PubMed](#)]
22. Wang, R.; Gu, X.; Li, Q.; Gao, J.; Shi, B.; Xu, G.; Zhu, T.; Tian, H.; Zhao, C. Aggregation Enhanced Responsiveness of Rationally Designed Probes to Hydrogen Sulfide for Targeted Cancer Imaging. *J. Am. Chem. Soc.* **2020**, *142*, 15084–15090. [[CrossRef](#)] [[PubMed](#)]
23. He, L.; He, L.H.; Xu, S.; Ren, T.B.; Zhang, X.X.; Qin, Z.J.; Zhang, X.B.; Yuan, L. Engineering of Reversible NIR-II Redox-Responsive Fluorescent Probes for Imaging of Inflammation In Vivo. *Angew. Chem. Int. Ed. Engl.* **2022**, *61*, e202211409. [[CrossRef](#)] [[PubMed](#)]
24. Lu, Z.; Tan, J.; Wu, Y.; You, J.; Xie, X.; Zhang, Z.; Li, Z.; Chen, L. NIR Light-Activated Mitochondrial RNA Cross-Linking Strategy for H₂S Monitoring and Prolonged Colorectal Tumor Imaging. *Anal. Chem.* **2023**, *95*, 17089–17098. [[CrossRef](#)] [[PubMed](#)]
25. Shortreed, M.; Kopelman, R.; Kuhn, M.; Hoyland, B. Fluorescent fiber-optic calcium sensor for physiological measurements. *Anal. Chem.* **1996**, *68*, 1414–1418. [[CrossRef](#)] [[PubMed](#)]

26. Zhao, H.; Qi, F.; Xiong, Y.; Lu, J. A chemiluminescent sensor for imaging endogenous hydrogen polysulfides in a living system. *Analyst* **2023**, *148*, 3347–3353. [[CrossRef](#)] [[PubMed](#)]
27. Sharma, N.; Kumar, V.; Jose, D.A. A ruthenium nitrosyl complex-based highly selective colorimetric sensor for biological H₂S and H₂S-NO cross-talk regulated release of NO. *Dalton Trans.* **2023**, *52*, 675–682. [[CrossRef](#)] [[PubMed](#)]
28. Wang, K.; Yang, X.; Guo, M.-Y.; Chen, X.-Y.; Li, T.; Yan, R.; Yang, Y.-S.; Zhu, H.-L.; Hu, Z.-G. Imaging the dynamic processes of hydrogen sulfide using a rapid “turn-on” mitochondria-targeting fluorescent probe. *Sens. Actuators B Chem.* **2022**, *369*, 132285. [[CrossRef](#)]
29. Zhang, C.L.; Liu, C.; Ding, Y.W.; Wang, H.T.; Nie, S.R.; Zhang, Y.P. A novel fluorescent probe based on naphthimide for H₂S identification and application. *Anal. Biochem.* **2023**, *677*, 115232. [[CrossRef](#)]
30. Du, Y.; Wang, H.; Zhang, T.; Wen, W.; Li, Z.; Bi, M.; Liu, J. An ESIPT-based fluorescent probe with fast-response for detection of hydrogen sulfide in mitochondria. *Spectrochim. Acta A Mol. Biomol. Spectrosc.* **2022**, *265*, 120390. [[CrossRef](#)]
31. Zeng, S.; Li, S.J.; Sun, X.J.; Li, M.Q.; Ma, Y.Q.; Xing, Z.Y.; Li, J.L. A naphthalene-quinoline based chemosensor for fluorescent “turn-on” and absorbance-ratiometric detection of Al³⁺ and its application in cells imaging. *Spectrochim. Acta A Mol. Biomol. Spectrosc.* **2018**, *205*, 276–286. [[CrossRef](#)] [[PubMed](#)]
32. Wang, L.; Li, W.; Zhi, W.; Huang, Y.; Han, J.; Wang, Y.; Ren, Y.; Ni, L. A new coumarin schiff based fluorescent-colorimetric chemosensor for dual monitoring of Zn²⁺ and Fe³⁺ in different solutions: An application to bio-imaging. *Sens. Actuators B Chem.* **2018**, *260*, 243–254. [[CrossRef](#)]
33. Chen, G.; Xu, J.; Zhan, Z.; Gao, X.; Jiao, M.; Ren, M.; Lv, L.; Chen, T.; Li, Y.; Liu, Y. A bright two-photon fluorescence probe with large stokes shift for deep tissue imaging of H₂S during metabolism. *Dye. Pigment.* **2020**, *172*, 107850. [[CrossRef](#)]
34. Liu, C.; Liu, Q.; Cai, S.; Ding, H.; He, S.; Zhao, L.; Zeng, X.; Gong, J. Novel near-infrared spectroscopic probe for visualizing hydrogen sulfide in lysosomes. *Spectrochim. Acta A Mol. Biomol. Spectrosc.* **2022**, *271*, 120917. [[CrossRef](#)] [[PubMed](#)]
35. Chen, X.; He, D.; Yang, X.; Yuan, F.; Yang, S.; Yang, Y.; Wang, K.; Qian, J.; Long, L. Construction of bifunctional fluorescent probe for two-step cascade recognition of hydrogen sulfide and biothiols in biological system. *Sens. Actuators B Chem.* **2023**, *381*, 133440. [[CrossRef](#)]
36. Zhu, J.; Hu, X.; Yang, B.; Liu, B. Dual sites fluorescence probe for hydrogen sulfide: AIEE activity and supramolecular assembly with β-cyclodextrin. *Sens. Actuators B Chem.* **2019**, *282*, 743–749. [[CrossRef](#)]
37. Ma, Y.; Wang, X.; Wang, Z.; Zhang, G.; Chen, X.; Zhang, Y.; Luo, Y.; Gao, G.; Zhou, X. A water-soluble NIR fluorescent probe capable of rapid response and selective detection of hydrogen sulfide in food samples and living cells. *Talanta* **2023**, *256*, 124303. [[CrossRef](#)] [[PubMed](#)]
38. Yang, Y.; Feng, Y.; Jiang, Y.; Qiu, F.; Wang, Y.; Song, X.; Tang, X.; Zhang, G.; Liu, W. A coumarin-based colorimetric fluorescent probe for rapid response and highly sensitive detection of hydrogen sulfide in living cells. *Talanta* **2019**, *197*, 122–129. [[CrossRef](#)] [[PubMed](#)]
39. Du, Y.; Wang, H.; Qin, L.; Zhao, M.; Pan, C. Rational development of an ESIPT-based fluorescent probe with large Stokes shift for imaging of hydrogen sulfide in live cells. *Bioorg Chem.* **2022**, *129*, 106158. [[CrossRef](#)]
40. Zhou, Y.; Yan, J.; Zhang, N.; Li, D.; Xiao, S.; Zheng, K. A ratiometric fluorescent probe for formaldehyde in aqueous solution, serum and air using aza-cope reaction. *Sens. Actuators B Chem.* **2018**, *258*, 156–162. [[CrossRef](#)]
41. Li, Y.; Chu, T.S. DFT/TDDFT study on the sensing mechanism of a fluorescent probe for hydrogen sulfide: Excited state intramolecular proton transfer coupled twisted intramolecular charge transfer. *J. Phys. Chem. A* **2017**, *121*, 5245–5256. [[CrossRef](#)] [[PubMed](#)]
42. Samanta, S.; Manna, U.; Ray, T.; Das, G. An aggregation-induced emission (AIE) active probe for multiple targets: A fluorescent sensor for Zn²⁺ and Al³⁺ & a colorimetric sensor for Cu²⁺ and F⁻. *Dalton Trans.* **2015**, *44*, 18902–18910. [[PubMed](#)]
43. Qin, X.; Liu, X.; Wang, J.; Chen, H.; Shen, X.C. A NIR ratiometric fluorescent probe for the rapid detection of hydrogen sulfide in living cells and zebrafish. *Talanta* **2024**, *266*, 125043. [[CrossRef](#)] [[PubMed](#)]
44. Xiong, J.; Xia, L.; Huang, Q.; Huang, J.; Gu, Y.; Wang, P. Cyanine-based NIR fluorescent probe for monitoring H₂S and imaging in living cells and in vivo. *Talanta* **2018**, *184*, 109–114. [[CrossRef](#)]
45. Ou, P.; Wang, Y.; Hao, C.; Peng, Y.; Zhou, L.Y. Naphthalimide-based a highly selective two-photon fluorescent probe for imaging of hydrogen sulfide in living cells and inflamed tissue of mouse model. *Spectrochim. Acta A Mol. Biomol. Spectrosc.* **2021**, *245*, 118886. [[CrossRef](#)]

Disclaimer/Publisher’s Note: The statements, opinions and data contained in all publications are solely those of the individual author(s) and contributor(s) and not of MDPI and/or the editor(s). MDPI and/or the editor(s) disclaim responsibility for any injury to people or property resulting from any ideas, methods, instructions or products referred to in the content.